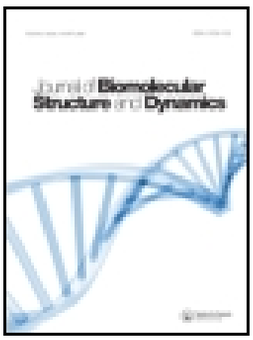

Taylor & Francis
Taylor & Francis Group

Journal of Biomolecular Structure and Dynamics

ISSN: 0739-1102 (Print) 1538-0254 (Online) Journal homepage: https://www.tandfonline.com/loi/tbsd20

Biomolecular interaction of a platelet aggregation inhibitor, 3,4-methylenedioxy-β-nitrostyrene with human serum albumin: Multi-spectral and computational characterization

Md. Zahirul Kabir, Amira Adlin Roslan, Nor Farrah Wahidah Ridzwan, Saharuddin B. Mohamad & Saad Tayyab

To cite this article: Md. Zahirul Kabir, Amira Adlin Roslan, Nor Farrah Wahidah Ridzwan, Saharuddin B. Mohamad & Saad Tayyab (2019): Biomolecular interaction of a platelet aggregation inhibitor, 3,4-methylenedioxy-β-nitrostyrene with human serum albumin: Multi-spectral and computational characterization, Journal of Biomolecular Structure and Dynamics, DOI: 10.1080/07391102.2019.1640133

To link to this article: https://doi.org/10.1080/07391102.2019.1640133

Accepted author version posted online: 04 Jul 2019.

Biomolecular interaction of a platelet aggregation inhibitor, 3,4-methylenedioxy-β-nitrostyrene with human serum albumin: Multi-spectral and computational characterization

Md. Zahirul Kabir[a], Amira Adlin Roslan[a], Nor Farrah Wahidah Ridzwan[b], Saharuddin B. Mohamad[b,c], Saad Tayyab[a,c*]

[a]Biomolecular Research Group, Biochemistry Programme, Institute of Biological Sciences, Faculty of Science, University of Malaya, Kuala Lumpur, Malaysia,

[b]Bioinformatics Programme, Institute of Biological Sciences, Faculty of Science, University of Malaya, Kuala Lumpur, Malaysia,

[c]Centre of Research for Computational Sciences and Informatics for Biology, Bioindustry, Environment, Agriculture and Healthcare, University of Malaya, Kuala Lumpur, Malaysia

Running Title: Platelet aggregation inhibitor binding to human serum albumin

***Corresponding author**

E-mail address: saadtayyab2004@um.edu.my (S. Tayyab).

Abstract

Molecular interaction of the 3,4-methylenedioxy-β-nitrostyrene (MNS), an inhibitor of platelet aggregation with the main transport protein, albumin from human serum (HSA) was explored using absorption, fluorescence and circular dichroism (CD) spectroscopy in combination with *in silico* analyses. The MNS–HSA complexation was corroborated from the fluorescence and absorption spectral results. Implication of static quenching mechanism for MNS–HSA system was predicted from the Stern-Volmer constant, K_{SV} - temperature relationship as well as the bimolecular quenching rate constant, k_q values. Stabilization of the complex was affirmed by the value of the binding constant (K_a = 1.48–0.56 × 10^4 M^{-1}). Thermodynamic data revealed that the MNS–HSA association was spontaneously driven mainly through hydrophobic interactions along with van der Waal's interaction and H-bonds. These results were well supported by *in silico* interpretations. Far-UV and near-UV CD spectral results manifested small variations in the protein's secondary and tertiary structures, respectively, while three-dimensional fluorescence spectra displayed microenvironmental fluctuations around protein's fluorophores, upon MNS binding. Significant improvement in the protein's thermostability was evident from the temperature results of MNS-bound HSA. Binding locus of MNS, as identified by competitive drug displacement findings as well as *in silico* analysis, was found to be located in subdomain IIA (Sudlow's site I) of the protein.

Keywords: 3,4-methylenedioxy-β-nitrostyrene; human serum albumin; ligand-protein interaction; fluorescence; *in silico* analysis

1. Introduction

Platelets are known to be involved in managing blood coagulation and regulating hemostasis (Yip, Shen, Berndt, & Andrews, 2005). Activation of glycoprotein GPIIb/IIIa (the main integrin of platelets) allows it to bind to fibrinogen with high affinity that might lead to platelets aggregation (Hsieh et al., 2010). 3,4-Methylenedioxy-β-nitrostyrene (MNS), whose structure is shown in the inset of Figure 1(A) is a promising inhibitor of tyrosine kinase and thus it blocks the activation of GPIIb/IIIa, and prevents platelet aggregation in blood circulation (Hsieh et al., 2010). MNS has shown higher efficiency compared to genistein in preventing protein tyrosine phosphorylation as well as platelet aggregation (Wang, Hsieh, Wu, & Wu, 2007).

Binding of a drug to HSA can substantially influence the drug properties, *i.e.*, distribution, clearance, elimination, efficiency and toxicity *in vivo* (Kragh-Hansen, Chuang, & Otagiri, 2002). The higher binding strength of a drug to the protein can reduce the free drug concentration from the blood, whereas low binding affinity may lead to its shorter lifetime (Kragh-Hansen et al., 2002). Therefore, drug–plasma protein interaction properties with respect to binding mode, binding constant and binding site(s) are vital to obtain information about the drug's pharmacokinetics, and hence are important in clinical as well as pharmacological applications (Zhang, Chen, Lu, Zhu, & Zhang, 2018). HSA is unique as the major transporter owing to its aptitude to bind reversibly the ligands with higher binding strength in comparison with other proteins present in plasma (Peters, 1996). Its three well-characterized binding sites I , II and III are positioned in subdomains IIA, IIIA and IB, respectively, assist in the binding of large number of ligands to the protein (Kragh-Hansen et al., 2002; Sudlow, Birkett, & Wade, 1975).

Many studies related to serum albumin-ligand interactions have been reported using various characterization tools such as spectrofluorimetry (Tunç, Duman, & Bozoglan, 2013a), equilibrium dialysis (Kosa, Maruyama, & Otagiri, 1997), UV-visible absorption spectroscopy (Tunç, Çetinkaya, & Duman, 2013b), circular dichroism (Duman, Tunç, & Bozoglan, 2013), Fourier-transform infrared spectroscopy (Tian, Liu, He, Hu, Yao, & Chen, 2004), isothermal titration calorimetry (Aki, & Yamamoto, 1994), potentiometry (Ayranci, & Duman, 2004a) and dynamic light scattering (Yu et al., 2011). However, due to certain limitations, some of these methods are not frequently used in ligand binding studies. For instance, equilibrium dialysis requires the analysis of free and total ligand concentrations and takes a long time. Lack of selectivity of ion selective electrodes for many ligands limits the use of potentiometric method in ligand-protein interaction studies (Ayranci, & Duman, 2004b). On the other hand, multi-spectroscopic approaches such as fluorescence, absorption and circular dichroism can provide useful information about protein-ligand interactions (Tunç, Duman, Soylu, & Bozoglan, 2014).

Although several studies, emphasizing the pharmacological importance of MNS, MNS–HSA interaction has not been explored yet. Therefore, to elucidate the molecular interactions between MNS and HSA, the present manuscript describes the effect of MNS binding on HSA spectral properties, detailed mechanism of the binding reaction, improvement in the protein's thermostability upon MNS binding and identification of the MNS binding sites in HSA.

2. Experimental

2.1. Reagents

Albumin from human serum (HSA; globulin and fatty acid free, lyophilized powder), phenylbutazone (PBZ), warfarin (WFN), ketoprofen (KTN) and hemin (HMN) were procured

from Sigma-Aldrich Co. (St Louis, MO, USA). MNS was supplied by Selleckchem (Houston, TX, USA). Other chemicals used in this study were of analytical standard.

2.2. Protein and drug solutions

HSA stock solution was prepared in 60 mM sodium phosphate buffer, pH 7.4 (PB 7.4) and its concentration was determined using spectrophotometric method (ε_m = 36 500 M^{-1} cm^{-1} at 280 nm) (Painter, Harding, & Beeby, 1998). A known amount (1.0 mg ml^{-1}) of MNS, WFN, PBZ, KTN and HMN crystals were mixed with dimethyl sulfoxide (DMSO) to prepare the stock solutions of drugs. Required dilutions of these solutions were made with PB 7.4 to prepare working solutions of the desired concentration. WFN concentration was determined using ε_m of 13 600 M^{-1} cm^{-1} at 310 nm (Twine et al., 2003).

2.3. Absorption spectra

The protein's (3 μM) absorption spectra (295–400 nm) without and with addition of rising MNS concentrations (6–48 μM with 6 μM increments) were recorded on Shimadzu UV-2450 spectrophotometer using quartz cuvettes (path length = 10 mm). The inner filter effect correction in the fluorescence spectra were made using these spectra.

In separate experiments, the absorption spectra (240–320 nm) of 25 μM HSA, MNS–HSA ([MNS]:[HSA] = 1:1, 4:1, 8:1, 12:1 and 16:1) mixtures and pure MNS solutions with similar concentrations were also collected.

2.4. Fluorescence spectra

The fluorescence spectra were registered on a Jasco spectrofluorometer (FP-6500 model) using a quartz cuvette (path length = 10 mm), containing the protein solution and positioning it in the thermostatically-controlled cell holder for 10 min for equilibrating the solution temperature.

In the titration experiments, the fluorescence spectra (310–400 nm) of HSA alone and with MNS were recorded using an excitation wavelength, λ_{ex} of 295 nm. All scanning parameters for fluorescence experiments were retained as described elsewhere (Kabir, Tee, Mohamad, Alias, & Tayyab, 2016).

The fluorescence spectra (360–480 nm) of WFN–protein and WFN–protein–MNS mixtures were collected using λ_{ex} of 335 nm.

The three-dimensional (3-D) fluorescence spectra of the protein (3 μM HSA) and MNS–protein mixtures ([MNS]:[HSA] molar ratio as 6:1 and 12:1) were obtained, following the same method as briefed earlier (Kabir et al., 2016).

2.5. Circular dichroism spectra

A Jasco spectropolarimeter (J-815 model) was employed for the measurement of the protein's circular dichroism (CD) spectra in the far-UV and near-UV regions under continuous nitrogen flow. The CD spectra of 3 μM (far-UV CD) / 5 μM (near-UV CD) HSA and MNS–HSA ([MNS]:[HSA] = 1:1) mixture were monitored in the same way as reported elsewhere (Tayyab, Francis, Kabir, Ghani, & Mohamad, 2019). Transformation of the measured ellipticity values to mean residue ellipticity (MRE, $deg.cm^2.dmol^{-1}$) was made, as suggested by Chen et al. (Chen, Yang, & Martinez, 1972).

The α-helical content of the protein (HSA) in the absence and with addition of MNS was calculated from the MRE_{208} value using the following equation (Lu, Cui, & Shi, 1987).

$$\alpha\text{-helix (\%)} = \left[\frac{(-\mathrm{MRE}_{208} - 4000)}{(33000 - 4000)}\right] \times 100 \quad (1)$$

2.6. MNS binding studies and fluorescence titration data analysis

The titration experiments were performed to obtain the binding characteristics of MNS–protein interaction following the published procedure (Kabir, Ghani, Mohamad, Alias, & Tayyab, 2018a). The protein concentration was kept at 3 μM, wheras MNS concentration was varied in the range, 6–48 μM (with 6 μM increments) in 3 ml incubation mixture. The samples were incubated separately at 288 K, 298 K and 308 K for 30 min for equilibrium establishment. After the fluorescence spectral measurements, the inner filter effect correction in the data was made using the following equation (Lakowicz, 2006).

$$F_{cor} = F_{obs} 10^{(A_{ex} + A_{em})/2} \quad (2)$$

where F_{cor} and F_{obs} are the corrected and the observed fluorescence intensity values, respectively. A_{ex} and A_{em} indicate the differences in the absorbance values of the protein (HSA) upon addition of MNS at the excitation wavelength (295 nm) and the emission wavelength (310–400 nm), respectively (Lakowicz, 2006).

The corrected fluorescence data of MNS−HSA system were treated in accordance with the published procedures (Feroz, Mohamad, Bakri, Malek, & Tayyab, 2013) to retrieve values of the Stern-Volmer constant (K_{SV}), the binding constant (K_a) and the bimolecular quenching rate constant (k_q) along with thermodynamic parameters, involved in the MNS–HSA interaction.

2.7. Thermal stability

The fluorescence intensity values at 342 nm ($FI_{342\ nm}$) of 3 μM HSA or MNS–protein ([MNS]:[HSA] = 6:1 and 12:1) mixtures were measured at different temperatures (298–353 K with an increments of 5 K) for analyzing the protein's thermal stability in the absence and upon addition of MNS, according to the procedure reported earlier (Kabir et al., 2018a).

2.8. Site marker-induced influences on MNS–HSA interaction

Different site markers, *i.e.*, WFN and PBZ (site I markers), KTN (site II marker) and HMN (site III marker) were selected as competitive probes in drug displacement investigations to identify the favored MNS binding location on HSA (Kragh-Hansen et al., 2002). In these experiments, the protein (3 μM HSA) or site marker–protein ([WFN] / [PBZ] / [KTN] / [HMN]:[HSA] = 1:1; previously incubated at 298 K for 30 min) mixtures were titrated with rising MNS concentrations (0–48 μM with an interval of 6 μM) and the fluorescence spectra were acquired after incubating the solutions for additional 30 min at 298 K. These spectra were scanned in the same way as described in Section 2.4.

2.9. Molecular docking

In silico approach was exploited to predict the binding orientation of MNS on the protein structure. The protein's crystallized structure (PDB ID: 1BM0; resolution: 2.5 Å) was collected from the Protein Data Bank, whereas MNS 3-D structure was constituted using Avogadro software (Hanwell et al., 2012). Analytical tools and other parameters for docking analyses were maintained the same as described in our previously-published report (Feroz et al., 2013). Interactions formed between MNS and the protein binding sites, *i.e.*, I, II and III were visualised and captured using UCSF Chimera (Pettersen et al., 2004). In addition, two-dimensional interaction maps between MNS and three binding sites of HSA were retrieved using LigPlot+

(Laskowski, & Swindells, 2011).

2.10. Statistical analysis

The obtained MNS–HSA interaction data were converted into the mean ± standard deviation (SD) in accordance with the mean value of three separate experiments. Statistical data processing, curve fitting as well as smoothing were made by exploiting the OriginPro 8.5 software (OriginLab Corp., Northampton, USA).

3. Results and discussion

3.1. Fluorescence titration results and binding constant of MNS-HSA interaction

Tryptophan (Trp) and tyrosine (Tyr) residues, present in proteins are the main contributor of intrinsic fluorescence that can be utilized to study ligand-induced protein's conformational changes as well as ligand-protein association (Lakowicz, 2006). Between two residues, Trp residues possess stronger fluorescence intensity due to the presence of indole group in their side chain (Chen, & Barkley, 1998). Therefore, HSA intrinsic fluorescence predominantly appears owing to its lone Trp (Trp-214) residue, when excited with an excitation wavelength (λ_{ex}) of 295 nm. However, Tyr fluorescence is relatively low at this wavelength due to energy transfer from Tyr to Trp residue (Lakowicz, 2006). Figure 1(A) displays the fluorescence quenching spectra of HSA, obtained upon addition of rising concentrations of MNS at 298 K. Characterization of the

fluorescence spectrum of HSA with an emission maximum (λ_{em}) of 342 nm was due to its single Trp residue, resided in the cleft of subdomain IIA of HSA (Peters, 1996). Inclusion of rising MNS concentrations in the reaction mixture led to a gradual reduction in the protein's fluorescence, showing ~32 % decrease at 48 μM concentration of MNS. However, these spectra were devoid of any shift in the λ_{em}. The decline in the protein's fluorescence intensity upon addition of MNS was suggestive of the MNS–HSA complexation, as resulted from the altered microenvironment around the Trp residue of HSA (Il'ichev, Perry, & Simon, 2002). Quantitatively, similar results were obtained at two other temperatures, *i.e.*, 288 and 308 K (Supplementary Figure 1).

Figure 1(B) shows the Stern-Volmer plots, obtained from the fluorescence data at three different temperatures, which obeyed the following straight line equations:

$F_0/F = 0.0145\ [MNS] + 1.0$ at 288 K

$F_0/F = 0.0094\ [MNS] + 1.0$ at 298 K

$F_0/F = 0.0055\ [MNS] + 1.0$ at 308 K

The K_{SV} values, as identified from the slope of these equations are listed in Table 1. Mechanisms of fluorescence quenching are categorized into either static or dynamic mode of quenching that can be individualized by the dependence of the K_{SV} value on temperature. Values of K_{SV} are assumed to reduce with rising temperature for the process of static quenching, whereas the opposite approach characterizes dynamic quenching (Lakowicz, 2006). The decreasing trend of K_{SV} (Table 1) with rising temperature anticipated the properties of static quenching in MNS-HSA system, hence suggested the formation of MNS–HSA complex. Values of k_q were obtained from the K_{SV} values after dividing it with τ_0 value, the fluorescence lifetime of HSA

(6.38×10^{-9} s) (Abou-Zied, & Al-Shihi, 2008). These k_q values (2.27×10^{12}, 1.47×10^{12} and 0.86×10^{12} M^{-1} s^{-1} for 288, 298 and 308 K, respectively) were greater than the maximum value (2.0×10^{10} M^{-1} s^{-1}) of dynamic quenching constant of a diffusion restricted process (Ware, 1962). Both these results characterized the MNS-induced quenching of protein fluorescence as static quenching and suggested the formation of MNS–HSA complex.

Values of K_a for MNS–HSA interaction were attained from the linear double log plots (Figure 1(C)) and are included in Table 1. The K_a values were found to remain in the range, $0.56–1.48 \times 10^4$ M^{-1}, indicating moderate nature of the protein's binding affinity towards MNS (Dufour, & Dangles, 2005). Such binding strength emerges suitable for the drug's efficient transport and its successive discharge at the target locus. It is noteworthy that the drug's affinity to the receptor at the target site is far greater compared to its affinity for proteins in plasma (Kragh-Hansen et al., 2002). Furthermore, the reducing trend of the K_a value with rising temperatures suggested the loss of strength in the MNS–HSA complexation at higher temperatures (Khalili, & Dehghan, 2019).

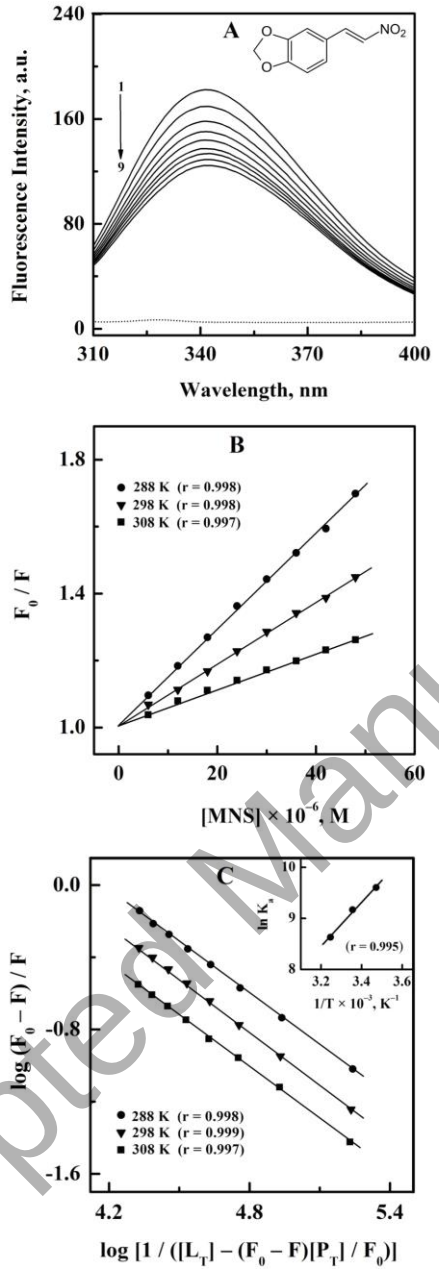

Figure 1. (A) MNS-induced fluorescence quenching results of 3 μM HSA in the absence (top spectrum) and upon addition of increasing (6–48 μM with 6 μM intervals) MNS concentrations (spectra 2–9), as studied in PB 7.4 at 298 K, using λ_{ex} of 295 nm. The fluorescence spectrum of free MNS (48 μM) is shown with dotted line. The 2-D structure of MNS is also depicted as insert. (B) Stern-Volmer plots and (C) Double logarithmic linear plots for MNS−HSA system, acquired at different temperatures, *i.e.*, 288 K, 298 K and 308 K. The inset (C) displays the van't Hoff plot for MNS−HSA interaction.

Table 1. Binding characteristics of MNS–HSA interaction, as obtained in PB 7.4 at three different temperatures.

T (K)	K_{sv} (M^{-1})	K_a (M^{-1})	ΔS (J mol^{-1} K^{-1})	ΔH (kJ mol^{-1})	ΔG (kJ mol^{-1})
288	$(1.45 \pm 0.12) \times 10^4$	$(1.48 \pm 0.16) \times 10^4$			-48.59 ± 0.15
298	$(0.94 \pm 0.09) \times 10^4$	$(0.96 \pm 0.11) \times 10^4$	$+44.35 \pm 0.18$	-35.82 ± 0.21	-49.04 ± 0.19
308	$(0.55 \pm 0.10) \times 10^4$	$(0.56 \pm 0.13) \times 10^4$			-49.48 ± 0.11

3.2. Acting forces associated with MNS–HSA interaction

Since fluorescence quenching revealed the dependence of K_a on temperature, the interaction of ligand with the protein seems to be a thermodynamic process. Therefore, parameters (ΔH, ΔS and ΔG) involving thermodynamics of MNS–HSA interaction were evaluated to anticipate the nature of forces associated in the binding reaction. Values of ΔS and ΔH, as acquired from the van't Hoff plot (inset of Figure 1(C)) along with the ΔG values at each temperature are also included in Table 1. The interaction of MNS with HSA was spontaneous and feasible at all studied temperatures as it was accompanied by the negative values of ΔG (Table 1). Four types of forces, which are predominantly involved in stabilizing ligand-protein complexes are hydrophobic interactions, electrostatic interactions, van der Waals forces and hydrogen (H)-bonds. The characteristic sign and magnitude of the thermodynamic parameters of ligand-protein interactions can differentiate among these forces (Ross, & Subramanian, 1981). While a positive ΔS value (+44.35 J mol^{-1} K^{-1}) is interpreted for the support of electrostatic and hydrophobic interactions, involvement of both van der Waals forces and H-bonds is reflected from the negative ΔH value (–35.82 kJ mol^{-1}) (Table 1) in MNS–HSA complex formation. However, role of electrostatic interactions in the binding process is excluded due to a large negative ΔH value; as electrostatic interactions are followed by a ΔH close to zero (Ross, & Subramanian, 1981). Therefore, forces such as hydrophobic interactions, van der Waals forces and H-bonds appear to favor the stabilization of the complex. Involvement of more than one forces in ligand-protein complex stabilization seems logical and has been reported in many ligand binding studies (Feroz et al., 2013; Li, Chen, Zhang, Duan, Yao, & Wei, 2017; Yeggoni, Rachamallu, Kallubai, & Subramanyam, 2015).

3.3. Absorption spectral analysis of MNS–HSA interaction

The absorption spectra were also used to support the fluorescence quenching results about MNS–HSA complex formation. Any change in the absorption spectrum of a protein upon ligand addition is usually translated as ligand binding to protein (Peters, 1996). Figure 2(A) displays the absorption spectra of HSA alone and upon inclusion of increasing MNS concentrations. These spectra were obtained after deducting the absorption contributions of pure MNS solution from the absorption spectra of MNS–HSA mixtures (Supplementary Figure 2). Emergence of the absorption peak at 278 nm demonstrated the contribution of protein's Trp and Tyr residues (Barreca, Lagana, Bruno, Magazu, & Bellocco, 2013; Makarska-Bialokoz, 2017; Makarska-Bialokoz, & Lipke, 2019). Enhancement of the absorption peak of HSA upon MNS addition clearly implied changes in the microenvironment around the protein's chromophores, which can be accounted for MNS–HSA complexation. Similar changes in the absorption spectrum of a protein have been shown in drug-protein binding studies (Kabir, Hamzah, Ghani, Mohamad, Alias, & Tayyab, 2018b; Li, Guo, Yan, Chen, Du, & Du, 2019; Makarska-Bialokoz, 2018).

3.4. Circular dichroism spectral analysis of MNS–HSA interaction

To evaluate the effect of MNS binding to HSA on its secondary and tertiary structures, the far-UV CD as well as the near-UV CD spectra of the protein and [MNS]:[protein] = 1:1 mixture were collected (Figure 2 (B) and (C)). As shown in the figure, pure MNS solution did not produce any CD spectral signal in the far-UV and the near-UV ranges. Emergence of two minima (λ = 208 nm and 222 nm) in the protein's far-UV CD spectrum projected the dominance of the α-helical structure in HSA (Figure 2(B)) (Bozoglan, Tunc, & Duman, 2014; Guercia, Forzato, Navarini, & Berti, 2016; Kelly, Jess, & Price, 2005). A small reduction in the MRE values at

these wavelengths upon inclusion of MNS in the solution mixture, indicated slight loss in the protein's α-helical content. Such difference in the far-UV CD spectra of HSA as well as MNS–HSA mixture apparently suggested protein's secondary structural variation due to MNS–HSA complex formation. Quantitatively, the α-helical content of HSA was reduced from 63 % to 55 % in the presence of MNS, which can be attributed to the alteration in the H-bonds network of the protein upon MNS binding (Zhang et al., 2011).

Similarly, the protein's near-UV CD spectrum was characterized by the presence of two minima (λ = 262 nm and 269 nm) and two shoulders (λ = 281 nm and 290 nm) (Figure 2(C)), which are ascribed to the disulfide bonds and aromatic chromophores in HSA (Kelly et al., 2005). However, slight alterations (reduced MRE values) in the CD spectrum of MNS–HSA mixture revealed tertiary structural changes brought about by MNS binding to the protein.

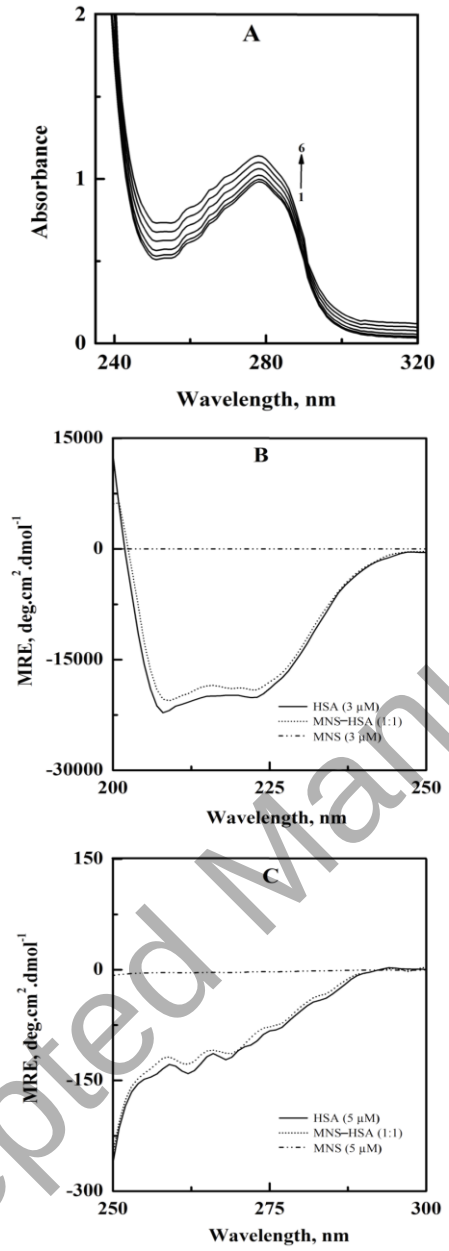

Figure 2. (A) UV-vis absorption spectra of 25 μM HSA (spectrum '1') and MNS:HSA mixtures in a molar ratio of 1:1, 4:1, 8:1, 12:1 and 16:1 (spectra 2–6), obtained in PB 7.4 at 298 K. (B) Far-UV CD and (C) near-UV CD spectra of the protein, free MNS and MNS–protein ([MNS]:[HSA] = 1:1) mixture, attained in PB 7.4 at 298 K. These spectra were acquired using the protein/MNS concentrations of 3 μM each and 5 μM each for far-UV CD and near-UV CD experiments, respectively.

3.5. Three-dimensional fluorescence spectral analysis of MNS–HSA interaction

Microenvironmental changes around HSA fluorophores induced by MNS binding were checked from the comparison of the 3-D fluorescence spectra of HSA and MNS–HSA mixtures. Figure 3 displays the 3-D fluorescence spectra and their contour maps of HSA (Figure 3(A)), [MNS]:[HSA] = 6:1 (Figure 3(B)) and [MNS]:[HSA] = 12:1 (Figure 3(C)) mixtures. The spectral characteristics in terms of peak position and fluorescence intensity are given in Table 2. Two scattering peaks, *i.e.*, the first-order (peak 'a'; $\lambda_{ex} = \lambda_{em}$) and the second-order (peak 'b'; $2\lambda_{ex} = \lambda_{em}$) peaks are frequently noticed with proteins (Lakowicz, 2006). The main peaks, *viz.*, peaks '1' (λ_{ex} = 280 nm) and '2' (λ_{ex} = 230 nm) reflect the fluorescence spectral features of the protein's Trp and Tyr residues (Lin, Liu, Chen, Huang, & Song, 2014). An appreciable loss in the intensity and blue shift in the λ_{em} of peaks '1' (~ 29%, 3 nm) and '2' (~ 64%, 12 nm) were seen upon inclusion of MNS to HSA solution ([MNS]:[HSA] = 6:1). Further reduction in the intensity values, showing loss of ~ 46% and ~ 72%, respectively, was observed at [MNS]:[HSA] molar ratio of 12:1. Such variations in these spectral characteristics clearly revealed distorted microenvironment around protein's fluorophores due to MNS–HSA complexation.

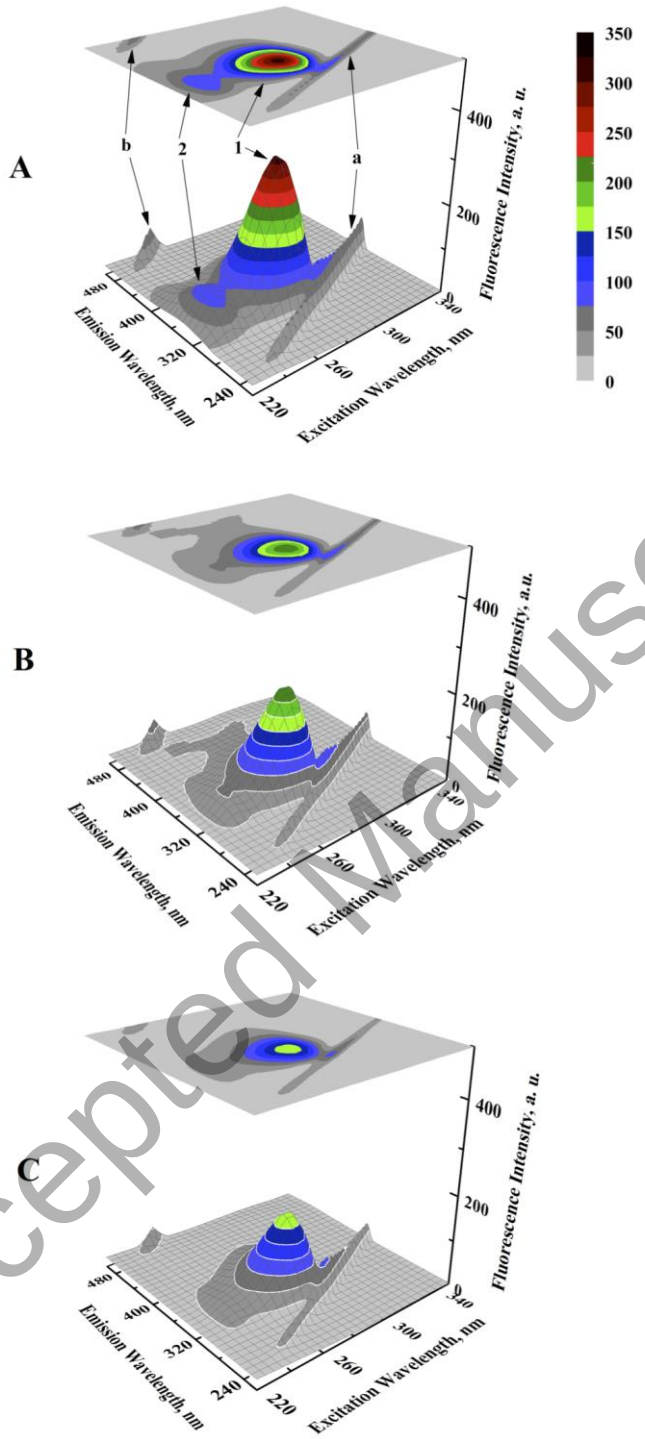

Figure 3. Three-dimensional fluorescence spectra and top contour maps of (A) 3 μM protein, (B) MNS–protein ([MNS]:[HSA] = 6:1) and (C) MNS–protein ([MNS]:[HSA] = 12:1) mixtures, as studied in PB 7.4 at 298 K.

Table 2. Spectral characteristics of three-dimensional fluorescence spectra of 3 μM HSA and MNS–protein ([MNS]:[HSA] = 6:1 and 12:1) mixtures, as obtained in PB 7.4 at 298 K.

System	Peak	Peak position [λ_{ex} / λ_{em} (nm/nm)]	Intensity
HSA	a	230/230→350/350	21.8→75.9
	b	250/500	72.7
	1	280/338	312.7
	2	230/335	83.5
[MNS]:[HSA] = (6:1)	a	230/230→350/350	20.2→60.2
	b	250/500	65.5
	1	280/335	220.8
	2	230/323	29.7
[MNS]:[HSA] = (12:1)	a	230/230→350/350	20.1→38.3
	b	250/500	53.0
	1	280/332	168.2
	2	230/328	23.6

3.6. Thermostability analysis of MNS–HSA interaction

Fluorescence spectroscopic technique has been employed to assess the improvement (if any) in proteins' thermal stability upon ligand binding (Feroz, Mohamad, Lee, Malek, & Tayyab, 2015; Sancataldo et al., 2014; Shi et al., 2012). In order to recognize the response of MNS–HSA complexation on protein's thermal stability, temperature-induced variations in the fluorescence intensity value at 342 nm ($FI_{342\ nm}$) of the protein as well as MNS–protein ([MNS]:[HSA] = 6:1 and 12:1) mixtures were studied and the results are presented in Figure 4. In both cases, gradual reduction in the $FI_{342\ nm}$ value was noticed with increasing temperature. However, relatively lesser decline in $FI_{342\ nm}$ value was registered with MNS–HSA mixtures (Figure 4). Quantitatively, 61% reduction in the $FI_{342\ nm}$ value was observed with HSA at 353 K compared to 49 % and 40 % loss with MNS–HSA mixtures at molar ratios of 6:1 and 12:1, respectively. Decrease in the $FI_{342\ nm}$ value with increasing temperature is the reflection of thermal denaturation of protein, which can change the environment around Trp residue from nonpolar to polar, thus resulting in the reduction in $FI_{342\ nm}$ (Il'ichev et al., 2002). In view of it, lesser decline in the $FI_{342\ nm}$ value with temperature suggested thermal stabilization of protein in the presence of MNS. MNS emerged to offer improved defense to the protein against temperature by forming more non-covalent bonds with the protein at its binding sites. Therefore, higher temperatures are required to destabilize these non-covalent bonds.

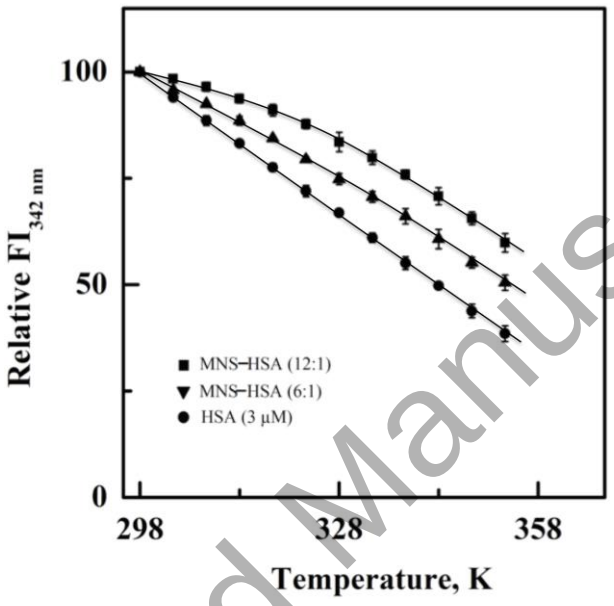

Figure 4. Plot showing comparison of thermal stability profiles of 3 μM protein and MNS–protein ([MNS]:[HSA] = 6:1 and 12:1) mixtures, as studied by fluorescence intensity measurements at 342 nm in PB 7.4 in the temperature range, 298–353 K at regular increments of 5 K.

3.7. Identification of MNS binding locus in HSA

Three well-recognized drug binding sites, namely, I, II and III have been projected in HSA owing to their greater affinity towards majority of drugs (Sudlow et al., 1975). Four well-known site-specific markers, *viz.*, WFN and PBZ (site I), KTN (site II) and HMN (site III) were used to identify the favored MNS binding locus on the protein (Kragh-Hansen, 1985; Kragh-Hansen et al., 2002).

The fluorescence spectra of WFN-HSA (1:1) mixture, obtained in the absence and upon inclusion of increasing MNS concentrations are presented in Figure 5(A). WFN–HSA complex showed the fluorescence spectra in the 360–480 nm range with an λ_{em} of 385 nm, when excited at 335 nm. The fluorescence intensity of WFN–HSA complex at the λ_{em} was gradually reduced with inclusion of increasing MNS concentrations to WFN-HSA mixture. Around 33 % loss in the fluorescence signal ($FI_{385\ nm}$) was registered at 48 μM MNS concentration (inset of Figure 5(A)). Such MNS-induced reduction in the $FI_{385\ nm}$ value of WFN–HSA complex was suggestive of the displacement of WFN from its binding site, *viz.*, Sudlow's site I due to MNS binding. However, pure WFN, MNS, HSA and MNS-HSA mixture did not produce any appreciable fluorescence signal in the same wavelength range (Figure 5(A)).

To further confirm the results obtained with WFN and exclude the possibility of MNS binding to Site II or site III, titrations of HSA and its complexes with PBZ, KTN and HMN were performed with rising MNS concentrations. These titration results are displayed in Figure 5(B). Although a progressive decline in the $FI_{342\ nm}$ value of the protein as well as site marker-HSA mixture was observed with increasing MNS concentrations, significantly smaller decrease in the $FI_{342\ nm}$ value was perceived with PBZ compared that noticed with HMN / KTN. In other words, PBZ offered more protection of site I towards MNS binding, which clearly suggested the

preference of MNS for Sudlow's site I of the protein. Furthermore, these titration results were transformed into the linear plots (Figure 5(C)) to determine the K_a values (Table 3) for MNS-HSA interaction, obtained with HSA and its complexes with PBZ, KTN and HMN. Reduction in the K_a value (Table 3) for MNS-HSA interaction was markedly greater with PBZ-HSA system, in comparison to that noticed with HMN / KTN-protein systems. Such decrease in the K_a value clearly indicated that presence of PBZ at site I significantly interfered the association of MNS with HSA, thus suggesting Sudlow's site I as the favored MNS binding locus in HSA. To validate the above findings, a site-specific molecular docking assessment was made, as discussed in Section 3.8.

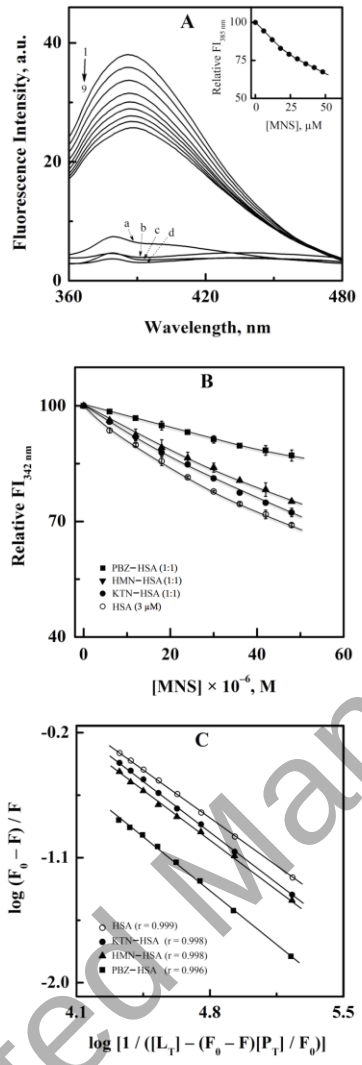

Figure 5. (A) Quenching of fluorescence spectra of WFN–HSA ([WFN]:[HSA] = 1:1; 3 μM each) mixture upon addition (top to bottom) of increasing (6–48 μM with 6 μM intervals) MNS concentrations. The spectra of 3 μM WFN (spectrum 'a'), 16:1 MNS:HSA mixture (spectrum 'b'), 3 μM HSA (spectrum 'c') and 48 μM MNS (spectrum 'd') are also included. These spectra were recorded in PB 7.4 at 298 K, using λ_{ex} of 335 nm. Inset dipicts the plot of relative $FI_{342\ nm}$ against [MNS]. (B) MNS-induced quenching in the relative $FI_{342\ nm}$ of HSA (3 μM) or site marker-protein ([PBZ]/[KTN]/[HMN]:[HSA] = 1:1) mixtures upon addition of increasing (6–48 μM with 6 μM intervals) MNS concentrations, as studied in PB 7.4 at 298 K, using λ_{ex} of 295 nm. (C) Double logarithmic plots for MNS−HSA interaction for the fluorescence data shown in Figure (B).

Table 3. Influence of different site-specific markers on the K_a values of MNS–HSA interaction, obtained in PB 7.4 at 298 K.

Site markers	K_a ($\times 10^3$ M^{-1})
–	9.62 ± 0.11
KTN	8.59 ± 0.17
HMN	6.79 ± 0.13
PBZ	3.87 ± 0.19

3.8. Molecular docking assessment of MNS–HSA interaction

Molecular docking assessment was executed for predicting atomic interactions formed between HSA amino acid residues and MNS at the respective binding sites, namely, I, II and III on the protein. Initial evaluation revealed that the most populated clusters at sites I, II and III were consisted of 91, 45 and 98 members, comprising the average binding energy of – 31.97, – 24.73 and – 28.08 kJ mol^{-1} (Figure 6(A)), respectively. On the other hand, values of the least binding energy calculated for MNS binding were – 32.09 kJ mol^{-1} (site I), – 24.90 kJ mol^{-1} (site II) and – 28.45 kJ mol^{-1} (site III). The best lowest binding energy (more negative) scored for Sudlow's site I clearly indicated that MNS was able to form more stable interactions with HSA at site I in comparison to site II or site III. Therefore, MNS preference is leaning towards site I compared to sites II / III of HSA.

MNS binding was further assessed using the lowest binding energy conformation generated on the sites I, II and III (Figure 6(B)). The formed complex at site I generated four H-bonds (Figure 6(C)), whereas two H-bonds were formed at both sites II (Figure 6(D)) and III (Figure 6(E)). The predicted H-bonds between connecting atoms of the protein's amino acid residues and MNS at each of the binding sites are included in Table 4. Apart from H-bonds formation, hydrophobic and polar interactions were also manifested from the LigPlots among other contributing factors towards the generated binding energy of MNS at all binding sites (Figure 7). Therefore, the docking analyses further anticipated that the MNS–HSA complex was stabilized by H-bonds and hydrophobic interactions, which further supported the above findings, discussed in Section 3.2.

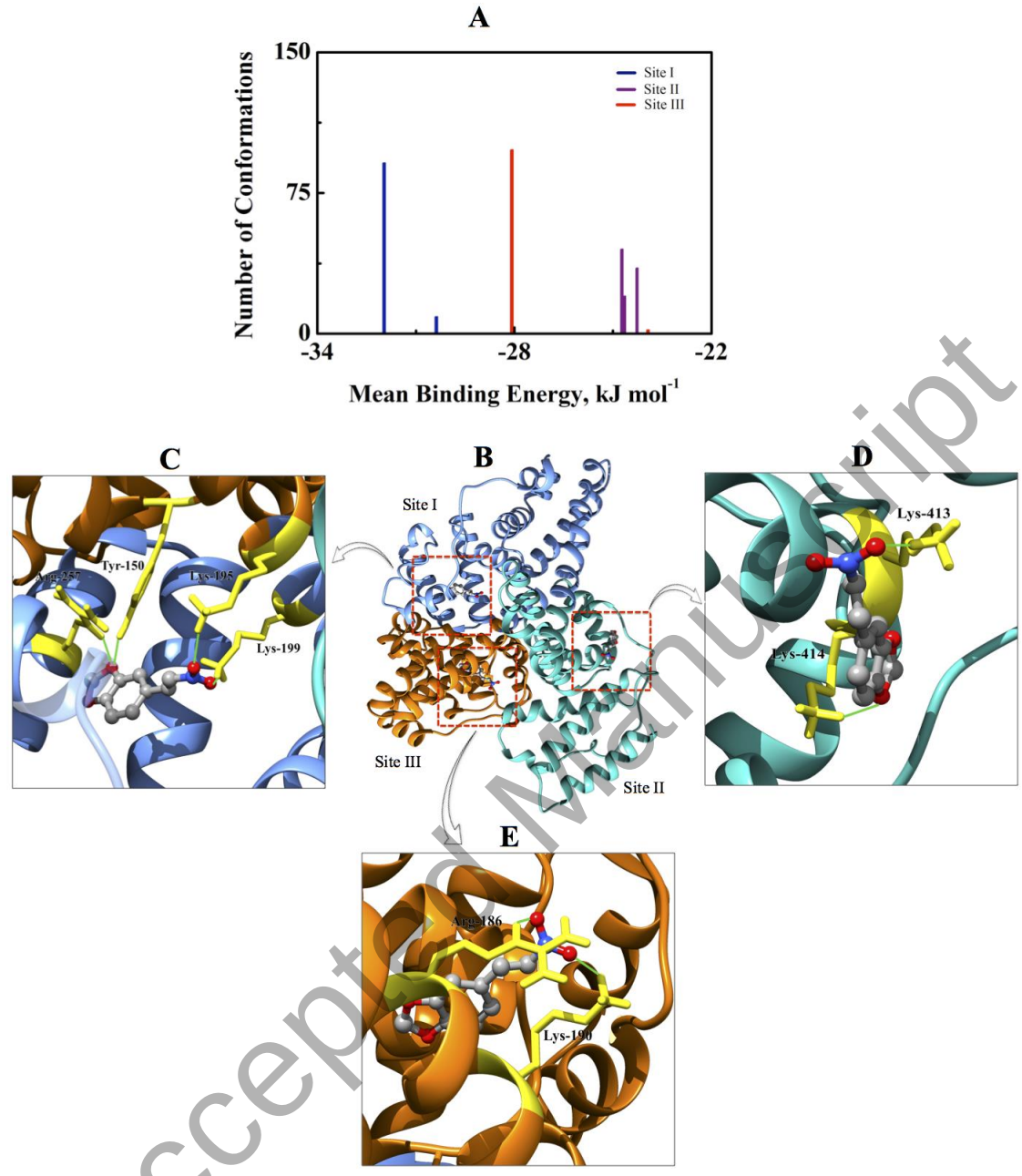

Figure 6. (A) Cluster analysis of the docking results of MNS−HSA interaction, as performed for the binding at sites I, II and III of HSA. (B) Predicted binding orientation of the lowest binding energy conformation of MNS (rendered in ball and stick) in HSA binding sites I, II and III. Domains of the protein are coloured in orange (domain I), blue (domain II), and green (domain III). Three binding sites were enlarged to manifest the formed hydrogen bonds (green lines) between the amino acid residues of HSA (rendered in yellow stick) and MNS at sites I (C), II (D) and III (E) of HSA.

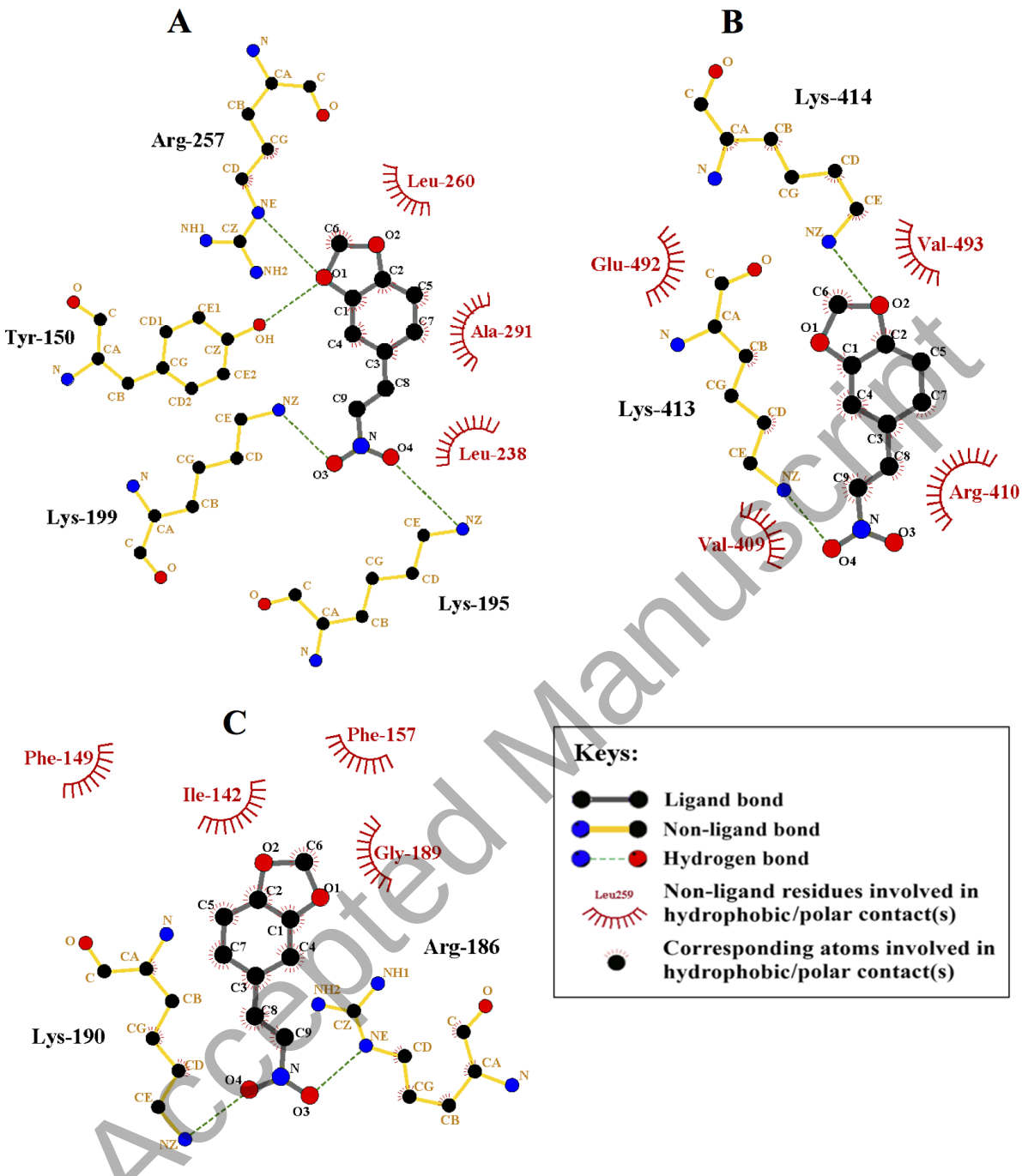

Figure 7. LigPlot+ diagrams representing the formed hydrophobic and polar interactions between MNS and HSA amino acid residues at three different binding sites, namely, I (A), II (B), and III (C) of the protein.

Table 4. Predicted hydrogen bonds formed between atoms of HSA amino acid residues and MNS at sites I, II and III, as obtained from the docking analysis.

HSA binding sites	HSA residue : atom	MNS atom	Distance (Å)
Site I	Tyr-150 : HH	O	2.12
	Lys-195 : HZ1	O	2.21
	Lys-199 : HZ1	O	1.96
	Arg-257 : HE	O	1.89
Site II	Lys-413 : HZ3	O	1.80
	Lys-414 : HZ2	O	1.93
Site III	Arg-186 : HE	O	2.11
	Lys-190 : HZ3	O	2.13

4. Conclusions

Interaction between MNS and HSA was found to be facilitated through moderate binding affinity ($K_a = 0.96 \times 10^4$ M^{-1} at 298 K), driven by favourable enthalpy and entropy changes ($\Delta H = -35.82$ kJ mol^{-1} and $\Delta S = +44.35$ J mol^{-1} K^{-1}) and stabilized by hydrophobic and van der Waal's forces along with hydrogen bonds. MNS binding to Sudlow's site I, located in subdomain IIA of HSA leads to slight alterations in the secondary and tertiary structures of the protein but added to its thermal stability.

Acknowledgements

The authors thank the Dean, Faculty of Science and the Head, Institute of Biological Sciences, University of Malaya for providing necessary facilities.

Disclosure statement

No potential conflict of interest was reported by the authors.

Funding

This work was financial supported by the University of Malaya Frontier Science Research Cluster (FRSC) [Frontier Research Grant (FRG) 2017 (FG025-17AFR)]. Md. Zahirul Kabir gratefully acknowledges financial assistance from the University of Malaya in the form of post-doctoral research fellowship.

References

Abou-Zied, O. K., & Al-Shihi, O. I. (2008). Characterization of subdomain IIA binding site of human serum albumin in its native, unfolded, and refolded states using small molecular probes. *Journal of the American Chemical Society*, *130*, 10793–10801.

Aki, H., & Yamamoto, M. (1994). Thermodynamic characterization of drug binding to human serum albumin by isothermal titration microcalorimetry. *Journal of Pharmaceutical Sciences*, *83*, 1712–1716.

Ayranci, E., & Duman, O. (2004a). Binding of lead ion to bovine serum albumin studied by ion selective electrode. *Protein and Peptide Letters*, *11*, 331–337.

Ayranci, E., & Duman, O. (2004b). Binding of fluoride, bromide and iodide to bovine serum albumin, studied with ion-selective electrodes. *Food Chemistry*, *84*, 539–543.

Barreca, D., Lagana, G., Bruno, G., Magazu, S., & Bellocco, E. (2013). Diosmin binding to human serum albumin and its preventive action against degradation due to oxidative injuries. *Biochimie*, *95*, 2042–2049.

Bozoglan, B. K., Tunc, S., & Duman, O. (2014). Investigation of neohesperidin dihydrochalcone binding to human serum albumin by spectroscopic methods. *Journal of Luminescence*, *155*, 198–204.

Chen, Y. H., Yang, J. T., & Martinez, M. (1972). Determination of the secondary structure of proteins by circular dichroism and optical rotatory dispersion. *Biochemistry*, *11*, 4120–4131.

Chen, Y., & Barkley, M.D. (1998). Toward understanding tryptophan fluorescence in proteins. *Biochemistry*, *37*, 9976–9982.

Dufour, C., & Dangles, O. (2005). Flavonoid–serum albumin complexation: Determination of binding constants and binding sites by fluorescence spectroscopy. *Biochimica et Biophysica Acta – General Subjects, 1721*, 164– 173.

Duman, O., Tunç, S., & Bozoglan, B. K. (2013). Characterization of the binding of metoprolol tartrate and guaifenesin drugs to human serum albumin and human hemoglobin proteins by fluorescence and circular dichroism spectroscopy. *Journal of Fluorescence, 23*, 659–669.

Feroz, S. R., Mohamad, S. B., Bakri, Z. S. D., Malek, S. N. A., & Tayyab, S. (2013). Probing the interaction of a therapeutic flavonoid, pinostrobin with human serum albumin: Multiplespectroscopic and molecular modeling investigations. *PLoS ONE, 8*, e76067.

Feroz, S. R., Mohamad, S. B., Lee, G. S., Malek, S. N. A., & Tayyab, S. (2015). Supramolecular interaction of 6-shogaol, a therapeutic agent of *Zingiber officinale* with human serum albumin as elucidated by spectroscopic, calorimetric and molecular docking methods. *Phytomedicine, 22*, 621–630.

Guercia, E., Forzato, C., Navarini, L., & Berti, F. (2016). Interaction of coffee compounds with serum albumins. Part II: diterpenes. *Food Chemistry, 199*, 502–508.

Hanwell, M. D., Curtis, D. E., Lonie, D. C., Vandermeersch, T., Zurek, E., & Hutchison, G. R. (2012). Avogadro: An advanced semantic chemical editor, visualization, and analysis platform. *Journal of Cheminformatics, 4*, 1–17.

Hsieh, P. W., Chang, Y. T., Chuang, W. Y., Shih, H. C., Chiang, S. Z., & Wu, C. C. (2010). The synthesis and biologic evaluation of anti-platelet and cytotoxic β-nitrostyrenes. *Bioorganic & Medicinal Chemistry, 18*, 7621–7627.

Il'ichev, Y. V., Perry, J. L., & Simon, J. D. (2002). Interaction of ochratoxin A with human serum al- bumin. A common binding site of ochratoxin A and warfarin in subdomain IIA. *Journal of Physical Chemistry B, 106*, 460–465.

Kabir, M. Z., Tee, W. V., Mohamad, S. B., Alias, Z., & Tayyab, S. (2016). Interaction of an anticancer drug, gefitinib with human serum albumin: Insights from fluorescence spectroscopy and computational modeling analysis. *RSC Advances, 6,* 91756–91767.

Kabir, M. Z., Ghani, H., Mohamad, S. B., Alias, Z., & Tayyab, S. (2018a). Interactive association between RhoA transcriptional signaling inhibitor, CCG1423 and human serum albumin: Biophysical and *in silico* studies. *Journal of Biomolecular Structure and Dynamics*, *36,* 2495–2507.

Kabir, M. Z., Hamzah, N. A. B., Ghani, H., Mohamad, S. B., Alias, Z., & Tayyab, S. (2018b). Biophysical and computational characterization of vandetanib–lysozyme interaction. *Spectrochimica Acta Part A: Molecular and Biomolecular Spectroscopy*, *189,* 485–494.

Kelly, S. M., Jess, T. J., & Price, N. C. (2005). How to study proteins by circular dichroism. *Biochimica et Biophysica Acta, 1751,* 119–139.

Khalili, L., & Dehghan, G. (2019). A comparative spectroscopic, surface plasmon resonance, atomic force microscopy and molecular docking studies on the interaction of plant derived conferone with serum albumins. *Journal of Luminescence*, *211,* 193–202.

Kosa, T., Maruyama, T., & Otagiri, M. (1997). Species differences of serum albumins: I. Drug binding sites. *Pharmaceutical Research, 14,* 1607–1612.

Kragh-Hansen, U. (1985). Relations between high-affinity binding sites of markers for binding regions on human serum albumin. *Biochemical Journal*, *225,* 629–638.

Kragh-Hansen, U., Chuang, V. T. G., & Otagiri, M. (2002). Practical aspects of the ligand-binding and enzymatic properties of human serum albumin. *Biological and Pharmaceutical Bulletin, 25,* 695–704.

Lakowicz, J. R. (2006). *Principles of Fluorescence Spectroscopy*. Third edn, Springer, New York.

Laskowski, R. A., & Swindells, M. B. (2011). LigPlot+: multiple ligand-protein interaction diagrams for drug discovery. *Journal of Chemical Information and Modeling, 51,* 2778–2786.

Li, Y., Chen, C., Zhang, C., Duan, J., Yao, H., & Wei, Q. (2017). Probing the binding interaction of AKR with human serum albumin by multiple fluorescence spectroscopy and molecular modeling. *Journal of Biomolecular Structure and Dynamics, 35,* 1189–1199.

Li, Y., Guo, Q., Yan, Y., Chen, T., Du, C., & Du, H. (2019). Different effects of *Forsythia suspensa* metabolites on bovine serum albumin (BSA). *Spectrochimica Acta Part A: Molecular and Biomolecular Spectroscopy, 214,* 309–319.

Lin, J., Liu, Y., Chen, M., Huang, H., & Song, L. (2014). Investigation on the binding activities of citalopram with human and bovine serum albumins. *Journal of Luminescence, 146,* 114–122.

Lu, Z. X., Cui, T., & Shi, Q. L. (1987). *Applications of Circular Dichroism and Optical Rotatory Dispersion in Molecular Biology*. First edn, Science Press.

Makarska-Bialokoz, M. (2017). Investigation of the binding affinity in vitamin B12-Bovine serum albumin system using various spectroscopic methods. *Spectrochimica Acta Part A: Molecular and Biomolecular Spectroscopy, 184,* 262–269.

Makarska-Bialokoz, M. (2018). Interactions of hemin with bovine serum albumin and human hemoglobin: A fluorescence quenching study. *Spectrochimica Acta Part A: Molecular and Biomolecular Spectroscopy, 193,* 23–32.

Makarska-Bialokoz, M., & Lipke, A. (2019). Study of the binding interactions between uric acid and bovine serum albumin using multiple spectroscopic techniques. *Journal of Molecular Liquids, 276,* 595–604.

Painter, L., Harding, M. M., & Beeby, P. J., (1998). Synthesis and interaction with human serum albumin of the first 3,18-disubstituted derivative of bilirubin. *Journal of Chemical Society, Perkin Transactions 1, 18,* 3041–3044.

Peters, T. (1996). *All About Albumin: Biochemistry, Genetics, and Medical Applications.* San Diego, CA: Academic Press.

Pettersen, E. F., Goddard, T. D., Huang, C. C., Cough, G. S., Greenblatt, D. M., Meng, E. C. & Ferrin, T. E. (2004). UCSF Chimera-a visualization system for exploratory research and analysis. *Journal of Computational Chemistry, 25,* 1605–1612.

Ross, P. D., & Subramanian, S. (1981). Thermodynamics of protein association reactions: Forces contributing to stability. *Biochemistry, 20,* 3096–3102.

Sancataldo, G., Vetri, V., Fodera, V., Cara, G. D., Militello, V., & Leone, M. (2014). Oxidation enhances human serum albumin thermal stability and changes the routes of amyloid fibril formation. *PLoS ONE, 9,* e84552.

Shi, S., Liu, J., Joshi, S. B., Krasnoperov, V., Gill, P., Middaugh, C. R., Volkin, D.B. (2012). Biophysical characterization and stabilization of the recombinant albumin fusion protein sEphB4–HSA. *Journal of Pharmceutical Sciences, 101,* 1969–1984.

Sudlow, G., Birkett, D. J., & Wade, D. N. (1975). The characterization of two specific drug binding sites on human serum albumin. *Molecular Pharmacology, 11,* 824–832.

Tayyab, S., Francis, J. A., Kabir, M. Z., Ghani, H., & Mohamad, S. B. (2019). Probing the interaction of 2,4-dichlorophenoxyacetic acid with human serum albumin as studied by experi- mental and computational approaches. *Spectrochimica Acta Part A: Molecular and Biomolecular Spectroscopy, 207,* 284–293.

Tian, J., Liu, J. He, W., Hu, Z., Yao, X., & Chen, X. (2004). Probing the binding of scutellarin to human serum albumin by circular dichroism, fluorescence spectroscopy, FTIR, and molecular modeling method. *Biomacromolecules, 5,* 1956–1961.

Tunç, S., Duman, O., & Bozoglan, B. K. (2013a). Studies on the interactions of chloroquine diphosphate and phenelzine sulfate drugs with human serum albumin and human hemoglobin proteins by spectroscopic techniques. *Journal of Luminescence, 140,* 87–94.

Tunç, S., Çetinkaya, A. & Duman, O. (2013b). Spectroscopic investigations of the interactions of tramadol hydrochloride and 5-azacytidine drugs with human serum albumin and human hemoglobin proteins. *Journal of Photochemistry and Photobiology B: Biology. 120,* 59–65.

Tunç, S., Duman, O., Soylu, I., & Bozoglan, B. K. (2014). Study on the bindings of dichlorprop and diquat dibromide herbicides to human serum albumin by spectroscopic methods. *Journal of Hazardous Materials, 273,* 36–43.

Twine, S. M., Gore, M. G., Morton, P., Fish, B. C., Lee, A. G., & East, J. M. (2003). Mechanism of binding of warfarin enantiomers to recombinant domains of human albumin. *Archives of Biochemistry and Biophysics, 414,* 83−90.

Wang, W. Y., Hsieh, P. W., Wu, Y. C., & Wu, C. C. (2007). Synthesis and pharmacological evaluation of novel β-nitrostyrene derivatives as tyrosine kinase inhibitors with potent antiplatelet activity. *Biochemical Pharmacology, 74,* 601–611.

Ware, W. R. (1962). Oxygen quenching of fluorescence in solution: An experimental study of the diffusion process. *The Journal of Physical Chemistry, 66,* 455–458.

Yeggoni, D. P., Rachamallu, A., Kallubai, M., & Subramanyam, R. (2015). Cytotoxicity and comparative binding mechanism of piperine with human serum albumin and α-1-acid glycoprotein. *Journal of Biomolecular Structure and Dynamics, 33,* 1336–1351.

Yip, J., Shen, Y., Berndt, M. C., & Andrews, R. K. (2005). Primary platelet adhesion receptors. *IUBMB Life*, *57*, 103–108.

Yu, M., Ding, Z., Jiang, F., Ding, X., Sun, J., Chen, S., & Lv, G. (2011). Analysis of binding interaction between pegylated puerarin and bovine serum albumin by spectroscopic methods and dynamic light scattering. *Spectrochimica Acta Part A: Molecular and Biomolecular Spectroscopy*, *83*, 453–460.

Zhang, G., Zhao, N., & Wang, L. (2011). Probing the binding of vitexin to human serum albumin by multispectroscopic techniques. *Journal of Luminescence, 131*, 880–887.

Zhang, J., Chen, L., Lu, D., Zhu, Y., & Zhang, Y. (2018). Interactions of pyrene and/or 1-hydroxypyrene with bovine serum albumin based on EEM-PARAFAC combined with molecular docking. *Talanta, 186*, 497–505.